UDC 621.224.7:532.52

VISUAL OBSERVATION OF INTERNAL FLOW THROUGH HIGH-HEAD PUMP-TURBINE

Takashi Kubota
Shoichi Kushimoto

I. Introduction

It is very important to investigate the flow stability in a reversible pump-turbine because a pump-turbine is more frequently operated in conditions outside the design range than a conventional hydro-turbine. A pump-turbine has hydraulic performance characteristics in which the optimum turbining head is inherently higher than the optimum pumping head [1]. Therefore, the operating head range in turbining mode normally becomes lower than the optimum turbining head, and in pumping mode the operating head range is apt to become higher than the optimum pumping head. As a result, both the low head turbining operation and high head pumping operation are apart from the respective optimum conditions, resulting in a tendency of unstable internal flow in a pump-turbine [2],[3]. Besides, a pump-turbine must frequently encounter transient unstable flows in the operating range well beyond the design values during frequent start and stop.

Heretofore, estimation of the flow stability was attempted in the model tests by measuring the dynamic data such as wall pressure pulsations, wicket gate torque fluctuations, dynamic radial thrust and noise, as well as the static hydraulic performance. In order to evaluate these static and dynamic data properly, however, it is necessary to ascertain through visual observations the internal flow patterns, particularly the flow separations, development of dead water zone, and stringy vortices on a boundary surface of normal/reverse flows.

A numerical experiment has recently become available for the internal flow through a pump-turbine by using flow analysis computer programs [4]. The computation can provide the flow pattern in the channels as well as the velocity and pressure distributions around the hydrofoils in a pump-turbine. The visualization of this information on the graphic display proves useful in comprehending the internal flow. Such an approach with a numerical experiment, however, is considered inapplicable to the unsteady flow far from the design operating range at present.

In the light of the above-mentioned necessity, greater demand is placed on a model pump-turbine for an in-depth visual observation of the internal flow pattern. In this case, a simplified configuration of a model pump-turbine may enable easy observation, but prevent establishing a relationship with the static and dynamic performance characteristics. A high-head model pump-turbine was built for performance tests by using transparent acrylic resin at part of it, and it served for both visual observation of the internal flow and measurements of static and dynamic characteristics for all four quadrants. Regarding the flow near the desing operating range, the observed flow patterns were compared with the results of computerized numerical experiments.

II. Test Arrangement and Method

1. Model pump-turbine

A model pump-turbine having low specific speed which was developed for a 500m head pumped storage power plant was adopted for the tests. Figure 1 shows the assembly sections and principal dimensions of the model unit. The large sized model unit facilitated visual observation of the internal flow. The right half of the figure shows the unit assembled to measure the static and dynamic hydraulic

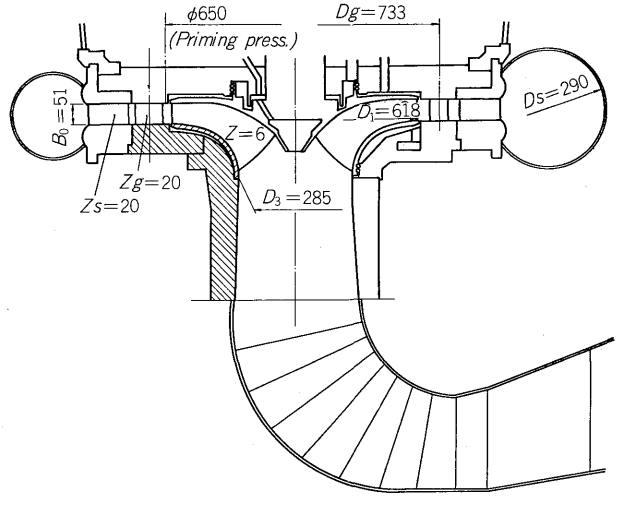

Fig. 1 Model pump-turbine

* This is the revised version of the paper with the same title which was presented to the IAHR-ASME-ASCE Joint Symposium on Design and Operation of Fluid Machinery held at Fort Collins (1978). Cf. Proceedings Vol. II. pp, 609-620.

characteristics. Hydraulic configurations of the model unit are completely homologous to those of the prototype machine including not only flow passages but also axial thrust relief pipes, runner chamber pressure equalizers, bottom cover drain holes, and air exhaust holes through the runner/head cover.

The left half of Fig. 1 shows the model assembled for visual observation of the internal flow. Runner band, bottom cover, discharge ring, and upper draft tube are made of transparent acrylic resin so that the flow patterns throughout the inside of the stay vanes can be observed visually.

2. Test arrangement and measuring instruments

The model pump-turbine was installed in a test stand in Fuji Hydraulic Laboratory to test the entire operating range covering the first through fourth quadrants. The flow rate through the model unit was measured digitally by an electromagnetic flowmeter calibrated by the gravimetric method, the rotating speed by a digital counter, the shaft torque by a beam balance digital torquemeter, and the upper and lower hydraulic pressures by digital mercury manometers.

Static digital data were acquired and processed statistically with a laboratory computer on-line. Computed results were printed out by a typewriter and stored in a magnetic tape to enable graphical post-processing by a large engineering computer. Dynamic analogue data were acquired through high speed A/D converter controlled by the computer to obtain the amplitude quickly, and stored in a data recorder for frequency analysis.

3. Test procedure

1) Performance test procedure

Test conditions for the respective four quadrants are shown in Table 1. For the flow of pumping direction (1 st and 4th quadrant), the impeller speed was kept constant (approx. 1,000 rpm) and the discharge and head were controlled by adjusting a valve downstream of the upper tank. On the other hand, the flow of turbining direction (2nd and 3rd quadrant) was tested by adjusting the runner speed with the head kept constant (approx. 60m).

2) Observation of internal flow

Internal flows through the model unit were observed visually under the same conditions as for the performance test, except that the head for the 3rd quadrant was reduced to 40m (Table 1). The light of a stroboscope was synchronized with the rotating speed to observe the internal flow pattern and take photographs. When necessary, a small amount of air was injected from the upstream side to facilitate the observation of the flow pattern. Furthermore, the transition of phenomena within an extremely short period was filmed with a high-speed camera (500~3,000 frames per second), which was projected at normal speed (24 frames per second) for the analytical observation.

Table 1 Test conditions

	1st	2nd	3rd	4th
n (rpm)	1,000	0 ~ 770	0 ~ 1,300	1,000
Q (l/s)	0 ~ 400	0 ~ 360	0 ~ 550	0 ~ 110
H (m)	45 ~ 75	40	60 (*40)	30 ~ 50
$Re=\frac{D_1\sqrt{2gH}}{\nu}$	1.8 ~ 2.4 $\times 10^7$	1.7×10^7	2.1×10^7 ($*1.7 \times 10^7$)	1.5 ~ 1.9 $\times 10^7$

*Condition for visual test.

3) Pump start test procedure

In order to observe the air exhaust/water filling process at pump start, with the wicket gates fully closed, the water around the rotating impeller was depressed by injecting compressed air through the air feed holes. Then the exhaust valve was opened to allow the depressed water level to rise, and the process of water filling in the priming chamber (a space between the wicket gates and impeller vane outer diameter) and in the impeller was observed. The leakage flow through the wicket gates during the water depression was measured by means of a turbine flowmeter with a throttle valve inserted into the leakage water supply pipe to the spiral case. The behaviour of the priming pressure, impeller input power and axial thrust during water filling was monitored and recorded on an oscillograph.

III. Flow Pattern in Normal Pump (First Quad.)

1. Pump inlet cavitation and reverse flow

Impeller inlet cavitation and reverse flow in the low discharge region affect most adversely the stability of the internal flow during the pump operation. Here the results of observation on these phenomena are described first. In order to establish an explicit relationship between the observed points and performance curves, first, all four quadrant characteristics of the model pump-turbine tested are illustrated in Fig. 2. The figure shows the four curves indicating flow rate-rotating speed with a parameter of gate

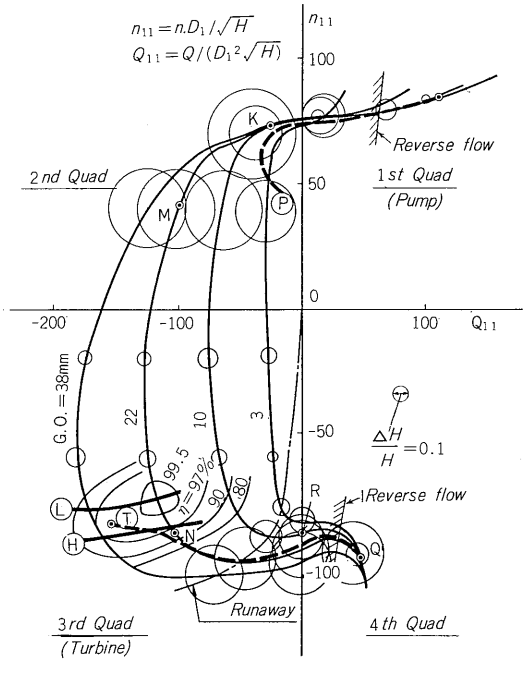

Fig. 2 Four-quadrant characteristics

opening (hereinafter abbreviated G.O.), with the unit discharge Q_{11} [$=Q/(D_1^2\sqrt{H})$] on the abscissa and unit speed n_{11} [$=n\cdot D_1/\sqrt{H}$] on the ordinate. Also illustrated are the amplitudes (peak-to-peak) of dynamic pressure in the priming chamber (refer to Fig. 1 for the measuring location) as related to the diameter of circles in Fig. 2, which is a typical measure for the flow stability. Test results for the lst quadrant are separately shown in Fig. 3 as the normal pump characteristic diagram. The diagram illustrates the curves indicating the total dynamic head H, pump efficiency η and impeller input power P versus discharge Q at several gate openings G.O.

While varying the pump inlet pressure (NPSH) and discharge, the incipient cavitation sigmas at which cavitation begins at the leading edge of impeller vanes were measured by visual observation as shown by the line②–⓪–① in the bottom of Fig. 3. In the high discharge region to the right of the minimum point ⓪ on the limit line for the cavitation inception, the relative flow angle (measured from the meridional line) at impeller inlet is smaller than vane inlet angle. This negative incidence angle may induce flow separation from the high pressure surface (hereinafter abbreviated H.P.S.) of the vane leading edge, resulting in an unstable flow pattern and increase in shock loss at impeller inlet. If the relevant operating sigma is below the incipient line ⓪–①, the cavitation develops on the H.P.S. from the band side having higher peripheral speed. Figure 4 shows a typical photo of the H.P.S. cavitation at point-A in Fig. 3. A triangular cavitation sheet is seen developing on the H.P.S. of the leading edge on this side of vanes at the outer periphery.

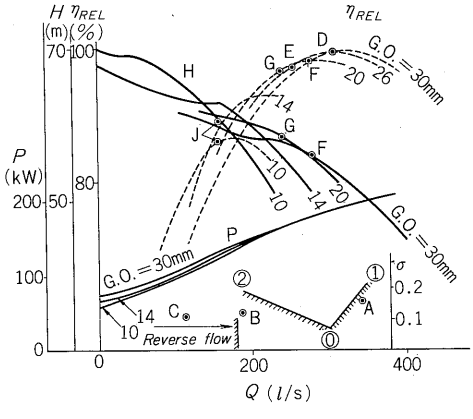

Fig. 3 Pumping characteristics.

In the low discharge region to the left of point ⓪, the relative flow angle becomes larger than the vane inlet angle. As a result of the positive incidence angle, the flow may separate from the low pressure surface (abbr. L.P.S.) of vane leading edge, disturbing the inlet flow pattern and increasing the shock loss. At the operating sigma below the incipient line ②–⓪, the cavitation develops from the L.P.S. of vane inlet. Figure 5 shows a photo of the L.P.S. cavitation at point–B in Fig. 3. Strip-like cavitation sheets are observed developing on the L.P.S. of leading edge on the other side of vanes.

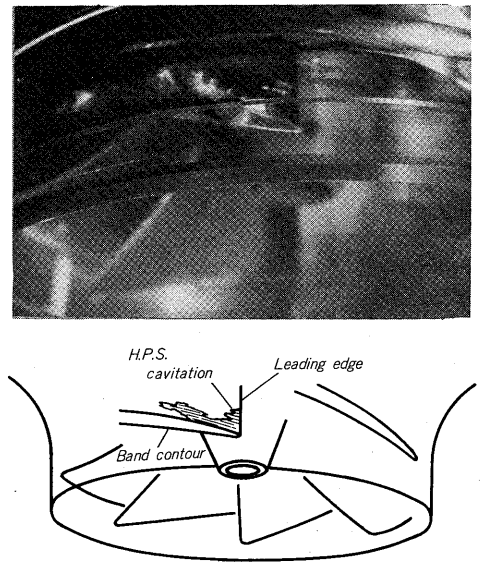

Fig. 4 H.P.S. cavitation at pump inlet (point-A)

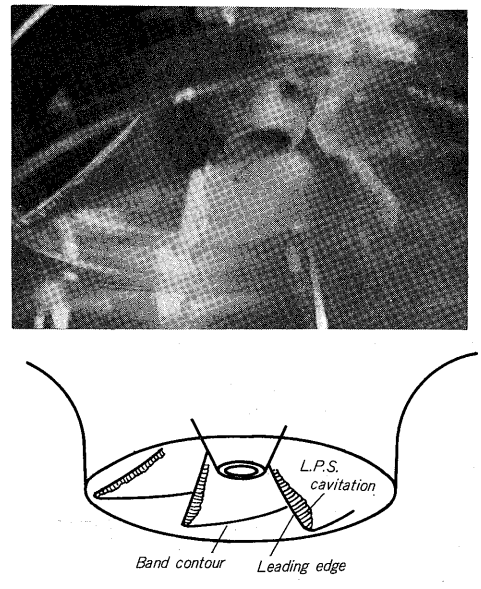

Fig. 5 L.P.S. cavitation at pump inlet (point-B)

At a nodal point ⓪ of the L.P.S. incipient line②–⓪ and H.P.S. line ⓪– ①, the relative flow enters into the impeller smoothly along the vane without shock, resulting in a cavitation-free and most stable inlet flow pattern. Accordingly, the impeller should be designed in such a way that the shock-free inflow point ⓪ locates at the middle of the operating range specified. In this sense, the determination of shock-free inflow point ⓪ from the above-mentioned cavitation observation becomes of great importance. However, the nodal point ⓪ cannot be obtained solely through the usual observation of L.P.S. cavitation, and the onset of H.P.S. cavitation must also be observed as demonstrated above.

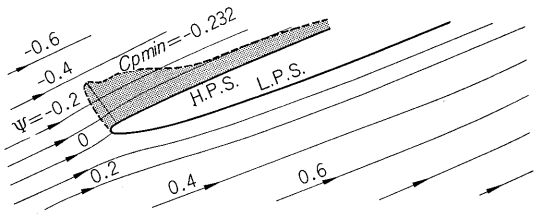

Fig. 6 Pressure distributions on H.P.S. of impeller inlet (point-A)

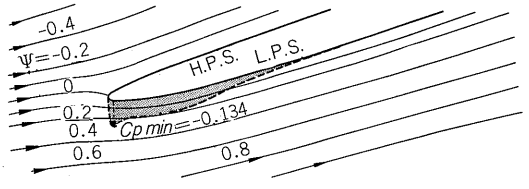

Fig. 7 Pressure distributions on L.P.S. of impeller inlet (point-B)

As a typical example of the computerized numerical experiments, Fig. 6 shows the pressure distributions on the vane surface and stream-lines around the leading edge of impeller vane in the high descharge range (point-A in Fig. 3). The lowest point of surface pressure appears on the H.P.S. turned round the leading edge. The computed incipient cavitation sigma (corresponding to the line ⓪– ①in Fig. 3) is obtained by changing the sign of pressure coefficient Cp [= $(Pmin-Pt_2)/(\gamma \cdot H)$] at the lowest pressure point. The computed result agrees well with the result (line ⓪– ①) observed in the model test. Figure 7 shows the result of the flow analysis in the low discharge range (point B in Fig. 3). Computed and observed results agree well with each other also in terms of incipient cavitation sigma on the L.P.S. of impeller vane. By executing the above computations for several flows, the shock-free inflow point can thus be determined numerically.

As the discharge is gradually reduced to about 60% of shock-free inflow discharge, the reverse flow occurs at impeller inlet [1]. A part of the water, which was sucked into the impeller along the crown side from the upper draft tube, was observed to turn round on the band side and return to the draft tube. The cavitation which developed on the L.P.S. of vanes along the leading edge line from band to crown so far disappears on the band side by sweeping away toward the upstream side. The fact that, at this moment, the cavitation on the crown side remains unaffected, reveals that the reverse flow is limited to the band side and the normal flow remains on the crown side. Once the reverse flow starts, the flow becomes unstable accompanying the rapid increase in hydraulic pressure pulsations (Fig. 2).

As the discharge decreases further, the area of reverse flow extends from the band side toward the crown along the leading edge line. Finally, the reverse flow dominates the whole impeller inlet when the discharge becomes zero (shut-off condition). Figure 8 shows a photo of strong reverse flow (point-C in Fig. 3) at the impeller inlet. A steep velocity gradient is formed on the boundary between the

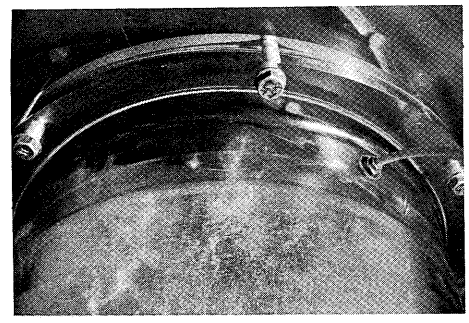

Fig. 8 Reverse flow at pump inlet (point-C)

normal flow on the crown side sucked from the center of upper draft tube and the reverse flow on the band side turned round to the periphery of upper draft tube. Cavitating vortex strings appear on this boundary plane and reach the upper draft tube carried away by the reverse flow. Figure 8 illustrates the upper draft tube becoming cloudy due to cavitating vortex strings. The swirl flow (i.e. pre-rotation) having the same direction as the impeller rotation appears in the upper draft tube due to the reverse flow. This low-discharge region of reverse flow is invariably encountered at every pump start and stop. In any case, the discharge of inicipient reverse flow has to be detected by the internal flow observations with a model test so as to avoid the normal operation in this range.

2. Rotating stall at diffuser inlet

When the discharge is reduced with G.O. kept constant (e.g. 26mm in Fig. 3), and it reaches a discharge (point-E in Fig. 3) slightly below the best efficiency point (point-D, and abbr., B.E.P.) for the relevant G.O., ultra-low frequency hydraulic pressure pulsations occur in the priming chamber (Fig. 9). The frequency of dynamic pressure is as low as 1/14 to 1/26 of impeller rotating frequency and its amplitude is relatively small. Accordingy, this dynamic pressure may often be overlooked in the measurement for a usual limited period. Propagating direction of the dynamic pressure is the same as the rotating direction of impeller. With decrease in G.O., the discharge at B.E.P. and thus the discharge at the start of ultra-low frequency dynamic pressure also decrease correspondingly. Figure 10 shows the results

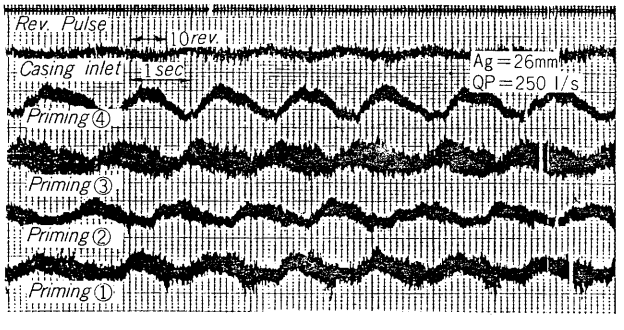

Fig. 9 Priming pressure fluctuations under the rotating stall (point-E)

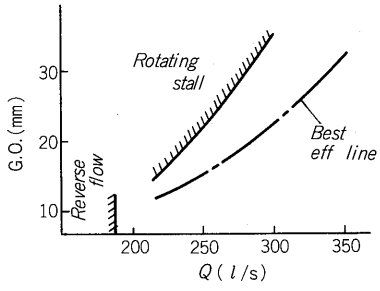

Fig. 10 Rotating stall region

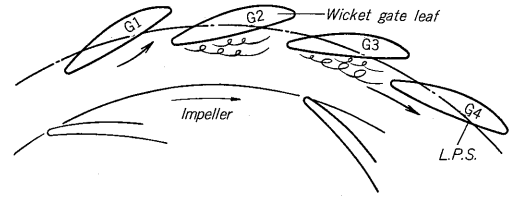

Fig. 11 Rotating stall at wicket gates

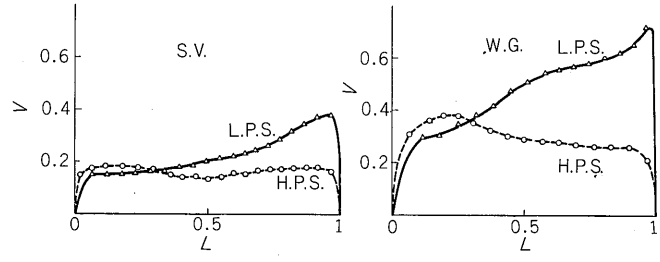

Fig. 12 Velocity distributions at large G.O. (point-F)

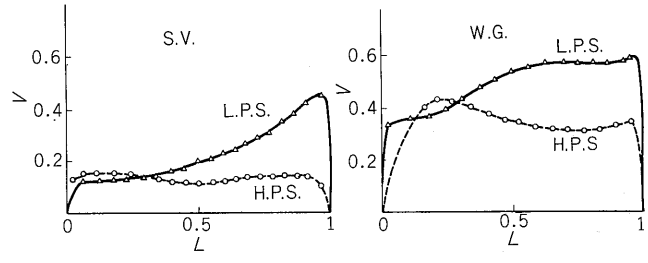

Fig. 13 Velocity distributions at small G.O. (point-G)

of measurement on the discharge at B.E.P. and the discharge of incipient ultra-low frequency dynamic pressure for each G.O.

These pressure fluctuations are attributable to the rotating stall at inlet of wicket gates and/or stay vanes. As the discharge decreases, the absolute flow angle measured from the meridian becomes larger at the impeller outlet. When the flow angle becomes larger than the inlet angle of gate leaf (i.e. high positive incidence angle), the flow separates from the L.P.S. of gate leaf (impeller side) causing stall of the gates and increase of hydraulic loss. Practically, however, all 20 gates can never stall simultaneously, and only a limited number of gates can stall at a time, producing so-called stall-cells (e.g. G2 and G3 in Fig. 11). This cell (separated flow region) blocks the upstream flow, raising its pressure. The flow keeping away from the cell enters the adjacent unstalled gate (G4 in Fig. 11) downstream of the cell at high speed and high incidence angle, resulting in this gate stalling. In the upstream region of cell, on the other hand, the incidence angle of flow eluding the cell becomes smaller (G1 in Fig. 11) which tends to prevent G2 from stalling. As a result, the stall-cell in G2-G3 is propagated to G3-G4 in the next instant. In conclusion, the stall-cell rotates very slowly in the flow direction (impeller rotating direction). Along with this, the stagnating pressure blocked by the cell is also put into slow rotation producing the ultra-low frequency priming pressure pulsations (Fig. 9).

Rotating stall at gate inlet can be presumed from the computerized numerical experiments. Figure 12 shows the computed velocity distributions around the wicket gates and stay vanes[4], when the rotating stall occurs (point-F in Fig. 3) at large G.O. (=30mm). Abscissa L shows the distance along the gate and vane surfaces (at pumping flow, L=1 for leading edge and L=0 for trailing edge). Since the flow enters the wicket gates with high positive incidence angle, the flow velocity is high at the L.P.S. of gate inlet and decelerates substantially toward the downstream. This means a high possibility of flow separation. Large G.O. results in a smaller flow angle discharging from gates, causing only a limited decelerating velocity at the L.P.S. of stay vane inlet.

Figure 13 shows the velocity distributions at a discharge (point-G in Fig. 3) where the rotating stall occurs at small G.O. (=20mm). As compared with Fig. 12, the gate deceleration is smaller, while the vane deceleration is larger. This is attributable to the small G.O. which in turn causes a small inflow angle to the stay vanes. Therefore, there is a possibility of rotating stall at the inlet of stay vanes when the G.O. is small. Furthermore, the rotating stall at stay vane inlet blocks the upstream flow to the wicket gates, resulting eventually in a rotating stall at the wicket gates.

In order to actually observe the rotating stall, a small volume of air was injected from the bottom of draft tube at point-J in Fig. 3 at small G.O. (=10mm). Figure 14 shows this photo in which the stall-cell on the L.P.S. (impeller side) of gate inlet appears whitish due to accumulating air. It was observed that these air bubbles propagated from gate to gate in the direction of impeller rotation along the wicket gate inlet.

In order to determine the number and rotating speed of stall-cells, a frequency analysis was executed by measuring the dynamic pressures on the walls of priming chamber circumferentially at four points having the same radius. The results reveal that the number of cells varies between two to four depending on the discharge. Correspondingly, the rotating speed of cells varies between 1/33 and 1/84 of impeller speed. At a certain low discharge, the number of cells varies between three and four from time to time and the

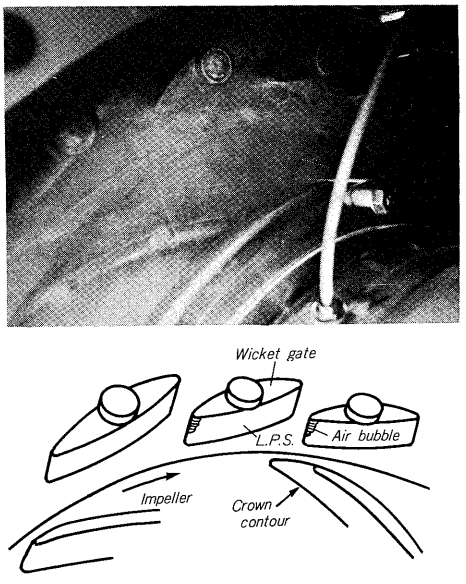

Fig. 14 Rotating stall at wicket gates (point-J)

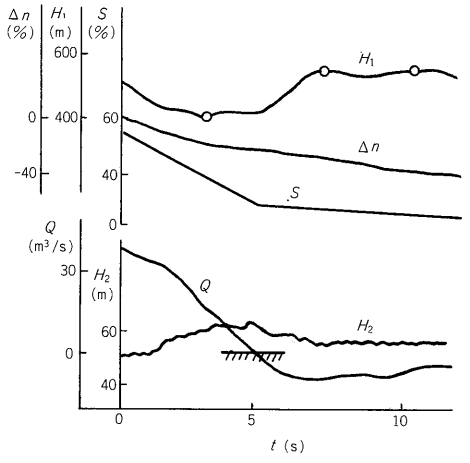

Fig. 15 Pump power failure

radial thrust on the impeller also varies substantially at that time. These phenomena will be detailed separately.

Only a few reports have been presented on the rotating stall at wicket gates and stay vanes as encountered during the pumping operation of pump-turbines[5]. It was confirmed that this phenomenon occurs not only in this model pump-turbine but also in other pump-turbines with different numbers and shapes of wicket gates and stay vanes regardless of specific speed. Though the rotating stall at diffuser inlet may tend to be overlooked because of its subtleness and ultra-low speed, careful consideration should be paid to avoid resonance with the natural frequency of penstock. Particular attention should be exercised in selecting the G.O. on cam for the high-head low-discharge operating range, because the rotating stall tends to occur at a lower discharge than B.E.P. at the relevant opening (cf. Fig. 10).

IV. Flow Pattern in Reverse Flow Pump (Second Quad.)

1. Reverse flow pump characteristics

Reverse flow pump characteristics are shown in the second quadrant of Fig. 2. This quadrant corresponds to the region transiently passed after a pump power failure. Figure 15 shows the transient characteristics in pump power failure from the min. head/max. power pumping operation. This was computed from the model pump-turbine complete characteristics in Fig. 2 by using the characteristic method computer program. Time is plotted on the abscissa, and plotted on the ordinate are the variation of spiral case pressure H1, draft tube pressure H2, speed variation △n, discharge Q and wicket gate servomotor stroke S. Circle marke on the H1 curve are to indicate, by the diameter, the amplitude (peak-to-peak) of pressure pulsations at the time concerned. Locus of power failure is indicated by a dash line Ⓟ in the 1st and 2nd quadrants on Fig. 2.

As is evident from the above, the pump power failure generally presents no particular problem in characteristics. If the wicket gates fail to close, however, even the slightest drop of impeller speed causes large variation in discharge within the transitory range from the lst to 2nd quadrant as shown in Fig. 2. Then the internal flow pattern undergoes excessive change within a short period. Once inside the 2nd quadrant, water flows toward the turbine direction in spite of the impeller still rotating in the pumping direction. This results in a turbulence in the flow from the wicket gates to runner outer diameter, causing noise and increased pressure pulsations. The results of visual observations are described below concerning the internal flow at point-K in the high pump speed/small turbine flow range and point--M in the low pump speed/large turbine flow range (both at G.O. =22 mm in Figure 2).

2. High pump speed/small turbine flow

At point-K in Fig. 2, the impeller rotates still at a considerably high speed and thus retains substantial centrifugal force, and only a small volume of water can overcome this force to flow toward the turbining direction. This water does not enter uniformly over the entire circumference; the turbining flow reaches only among three to four wicket gates and there is almost no through-flow among the remaining 16 to 17 gates. A large cell blocking the turbining flow (as well as the remaining flow region) does not stand still. It was observed that the cell propagated from gate to gate, and thus rotated slowly in the direction of impeller rotation, as in the case of rotating stall during the pumping operation.

Figure 16 is a photo showing a part (transparent portion to the left) of the large block cell produced between the wicket gates and impeller outer diameter as well as the turbining flow region (whitish portion to the right). Though the air is injected from the upstream side of stay vanes, it does not enter the blocked cell, leaving the transparent cell portion in the photo. In the space inside of gates, the flow

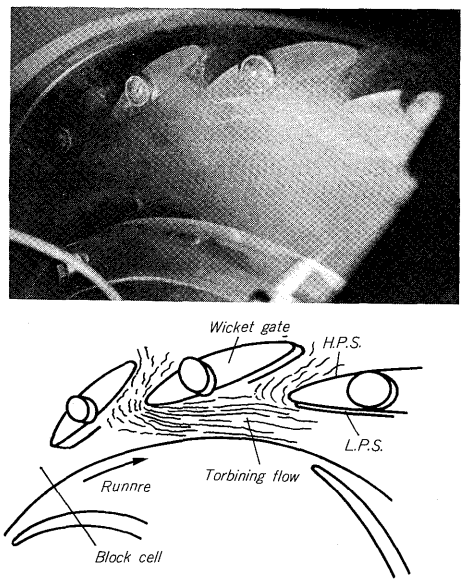

Fig. 16 High pump speed/small turbine flow (point-K)

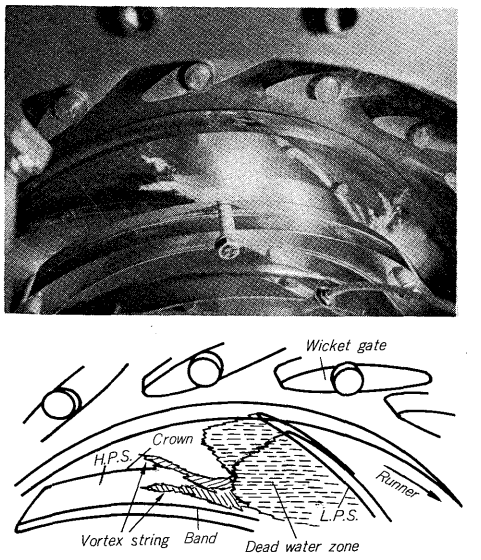

Fig. 18 Low pump speed/large turbine flow (point-M)

separates from the L.P.S. of gates under the strong swirl flow (directing left to right in Fig. 16) discharged from the impeller. On the other hand, the turbining flow region where air bubbles concentrate appears whitish in Fig. 16. After passing through the wicket gates, the turbining flow goes round the trailing edge of gate and is bent at a sharp angle toward the impeller rotation (clockwise) under the strong swirl flow. Observation proved that the flow region of air concentration propagated from gate to gate, resulting in a slow rotation. In this condition, obviously, the radial thrust acting on the impeller fluctuates heavily with a very low frequency.

3. Low pump speed/large turbine flow

At point-M in Fig. 2, the impeller speed drops and the pumping effect by centrifugal force becomes less dominant. Water enters stably through the wicket gates into the runner in the turbining direction. Figure 17 shows the velocity triangle at the runner inlet calculated from the mean flow rate. The flow enters the runner vanes at an extremely large incidence angle and separates excessively from the leading edge. As shown in Fig. 18, a wide dead water zone develops over the L.P.S. of the vane covering nearly the entire flow passage. Water flows, at high velocity, through a narrow region along the H.P.S. of the adjacent vane forming a plane of steep velocity gradient on the boundary with the dead water zone. It was observed that two bold vortex strings appeared along the H.P.S. in the corner between the band (on this side of photo) and crown (farther side).

V. Flow pattern in Normal Turbine (Third Quad.)

Turbine performance characteristics are shown in the third quadrant of Fig. 2 with the hill chart of relative efficiency. When the unit speed n_{11} increases above the optimum speed, the unit discharge Q_{11} decreases gradually and drops suddenly around the runaway speed. This is the discharge-speed characteristics inherent in the pump-turbine having a low specific speed. In the region after the sharp fold of n_{11}-Q_{11} curves, the turbine efficiency deteriorates rapidly and pressure pulsations in the priming chamber and dynamic torque of wicket gates increase suddenly [3].

Critical operating conditions, under which the cavitation starts at the runner vane inlet, were determined from the visual observation and are shown by lines Ⓛ and Ⓗ in Fig. 2. Within the range above the critical line Ⓛ, the flow

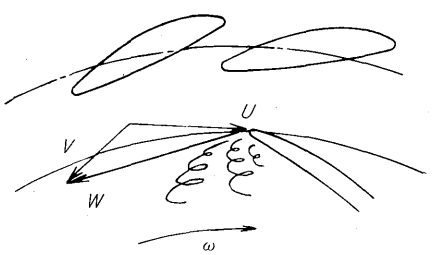

Fig. 17 Velocity triangle at runner inlet (point-M)

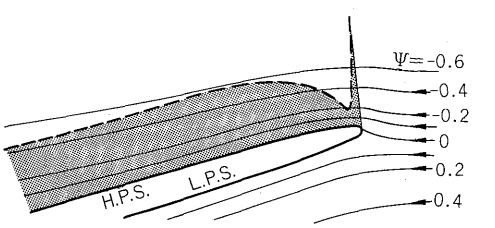

Fig. 19 Pressure distributions at runner inlet (point-N)

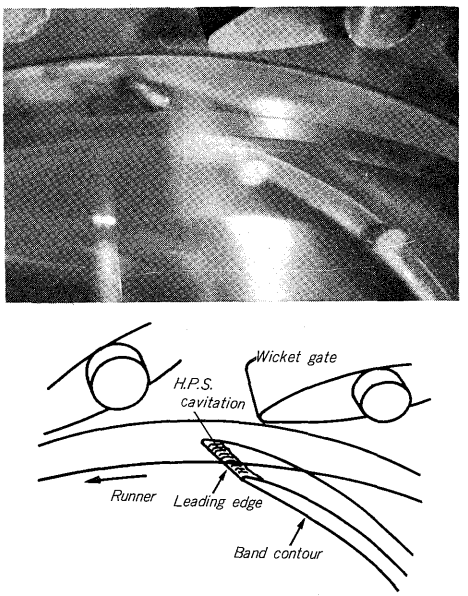

Fig. 20 Cavitation at runner inlet (point-N)

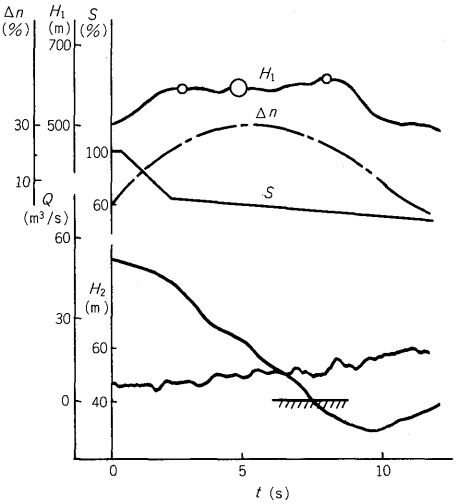

Fig. 21 Turbine load rejection

enters at an angle (measured from the meridian) smaller than the vane leading edge angle to cause cavitation due to flow separation from the L.P.S. of leading edge, resulting in unstable flow. Similarly, within the range below the line Ⓗ, the flow angle is larger than the leading edge angle, causing cavitation on the H.P.S. and thus resulting in disturbed flow. Figure 19 shows the computerized pressure distribution on the H.P.S. and streamlines around the vane inlet at point-N in Fig. 2. The negative pressure peak comes to the point on the H.P.S. going round the leading edge, at which the flow would separate. Figure 20 shows the H.P.S. cavitation at the runner inlet at point-N in Fig. 2. As the relative position between the runner vane leading edge and wicket gate trailing edge changes with the runner rotation, the degree of H.P.S. cavitation development varies cyclically. The increase of priming pressure pulsation and noise, which are encountered when G.O. is decreased during the low head (high n_{11}) turbining operation, is attributable to this H.P.S. flow separation. Thus it is essential to measure cavitation incipient lines Ⓛ and Ⓗ through visual observation in order to determine the stable turbining operation range.

With regard to the flow pattern in the third quadrant, further observation is necessary on the behaviour of the cork-screw vortex core which is developed in the upper draft tube due to the swirl flow discharged from the runner[6]~[8]. It is especially important to evaluate the stability of partial and heavy load operations, and transitory pressure pulsations in the draft tube after the load rejection. Detailed explanations of these flow patterns will be left for another occasion.

VI. Flow Pattern in Reverse-RPM Pump (Fourth Quad.)

1. Reverse-RPM pump characteristics

The reverse-RPM pump characteristics are shown in the fourth quadrant of Fig. 2. The n_{11}-Q_{11} curves enfold remarkably from the third to fourth quadrant, showing a strong S-curve characteristic inherent to the low specific speed pump-turbine. This range is transiently passed after the load rejection. Figure 21 shows the transient characteristics when the turbine load is rejected from the full-load operation at a rated head. Calculation method and graphical illustrations are the same as for the pump power failure in Clause 1 of Chapter IV. The locus of the transient characteristics is shown by dashed line Ⓣ in the third to fourth quadrant of Fig. 2. The slight variation in rotating speed of pump-turbine causes large variation in discharge near the runaway speed, resulting in increased pressure rise. Besides, the S-curve characteristics tend to lead the turbining operation into the fourth quadrant.

In the case of reverse-RPM pump, unlike the normal pump, water is pumped up by the impeller rotating in the turbining direction. Accordingly, the inflow conditions are greatly deteriorated at the impeller and wicket gate inlets, accelerating the priming pressure pulsations and wicket gate dynamic torque (cf. Fig. 2). Described below are the results of observation on the internal flow pattern at point-Q (max. discharge of reverse-RPM pump) and at point-R (zero flow rate) on the locus Ⓣ in Fig. 2.

2. Flow in large discharge region

Figure 22 shows the velocity triangles at impeller and wicket gate inlets at point-Q in Fig. 2. At the impeller inlet, the relative flow W_2 enters at an angle extremely deviated from the vane leading edge angle, causing flow separation from the H.P.S. of leading edge and thus producing a wide dead water zone along the H.P.S. of vanes. The hydraulic shock loss at impeller inlet is very large. Figure 23 shows a photo of the cavitating dead water zone on the H.P.S. of impeller inlet. The dead water zone can be seen to heap up on the vane and extend from the leading edge over to the upstream side. The water approaching the leading edge goes round the dead water zone, and flows through a very narrow passage along the L.P.S. of adjacent vane. On the band

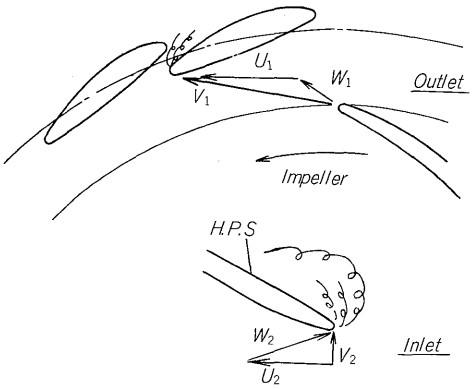

Fig. 22 Velocity triangles at impeeler inlet/outlet (point-Q)

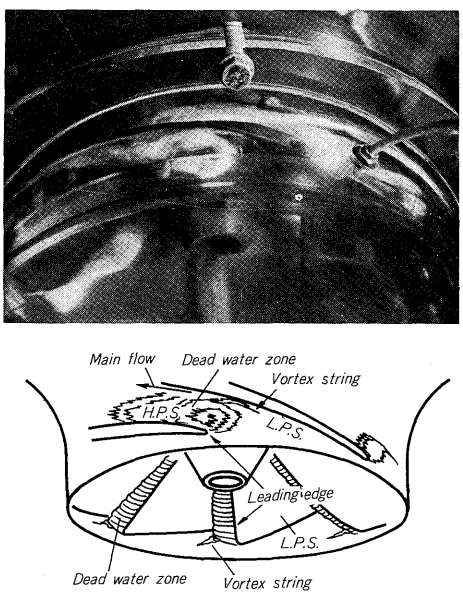

Fig. 23 Flow separations at impeller inlet (point-Q)

side of inlet throat in the vane passage, a cavitating vortex string is seen developing from the plane of velocity gradient on the boundary between the main flow and the dead water zone. At the impeller inlet, the flow is normal (pumping flow) over the entire leading edge line from crown to band. No reverse flow can be observed toward the draft tube. Due to the strong flow separations from the leading edge, however, the flow is disturbed accompanied by large noise.

Water flow discharging from the impeller has a strong absolute swirl flowing in the same direction as the impeller rotation, as shown by V_1 in Fig. 22. This high velocity water must change its direction suddenly at the gate inlet and flows into the gate throat. Then the flow separates from the H.P.S. of leading edge to cause cavitation and large hydraulic loss. The flow pattern in this condition is shown in the photo of Fig. 24. In the gate throat of the bottom cover side the cavitating vortex string can be seen. This flow separation in the gate throat is attributable to the increase of dynamic gate torque which is produced after the load rejection during the reverse-RPM pump operation[2].

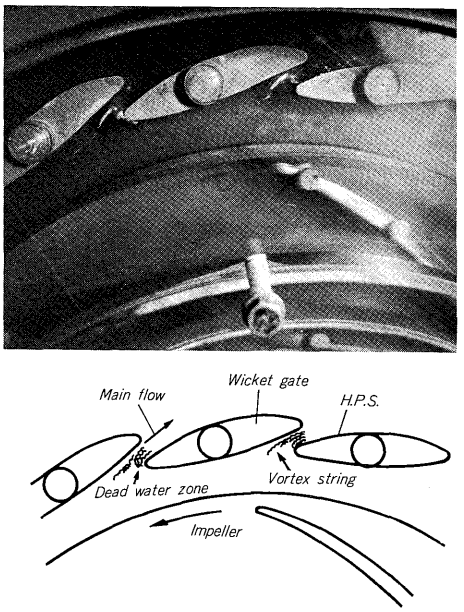

Fig. 24 Flow separations at wicket gates (point-Q)

3. Flow in small discharge region

As in the case of a normal pump, the reverse-RPM pump also suffers a reverse flow at the impeller inlet as the discharge decreases. Figure 25 shows the reverse flow at impeller inlet at point-R in Fig. 2. The cavitating dead water zone remaining on the crown side of leading edge line reveals that water is still sucked in from the crown side. Part of the sucked water reverses direction on the band side and flows into the draft tube. This is evidenced by the fact that the dead water zone is completely blown off on the band side. As the discharge approaches zero, the flow pattern becomes quite similar to that in the braking zone in the third quadrant. There is a strong re-circulating flow in the priming chamber between the impeller outlet and gate

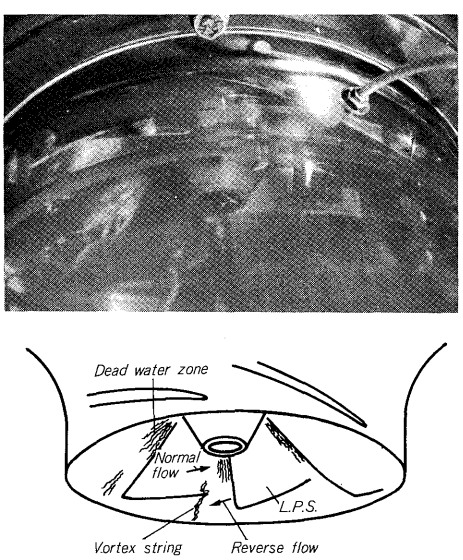

Fig. 25 Reverse flow at impeller inlet (point-R)

inlet, as well as the dominant reverse flow at impeller inlet with the heavy pre-swirl having the same direction as impeller rotation.

VII. Flow Pattern during Pump Start

1. Flow under water depression

Generally, the Francis pump-turbine is started by rotating the impeller in the air after the depression of water with the wicket gates fully closed, in order to decrease the pump starting input power. In this case, the leakage water from wicket gates, if admitted into the impeller, will increase the input power. The spiral casing pressure has to be reduced to minimize the leakage flow, and water draining is necessary from the outer periphery of runner band chamber to prevent leakage water from entering the impeller. To confirm the effectiveness of these preventive measures, the input power in the air was measured while making a visual observation of internal flow pattern.

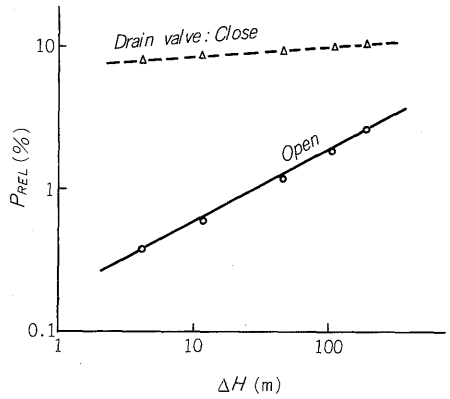

Fig. 26 Impeller input in the air

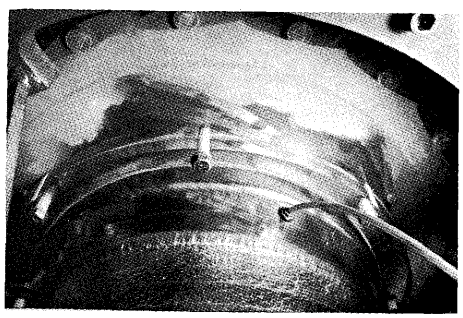

Fig. 27 Drain valve closed

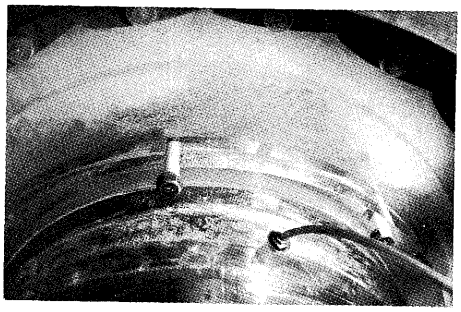

Fig. 28 Drain valve open

Figure 26 illustrates the measured impeller input in the air for the opening and closing of runner band drain valve. In the figure, the differential pressure ΔH between the spiral case and priming chamber is taken on the abscissa and the ratio P_{REL} of impeller input power in the air to the rated pump input power on the ordinate. Water volume leaked from the wicket gates is proportional to a square root of differential pressure ΔH. With the runner band drain valve closed, the impeller input was measured to about 9% of rated pump input. This large impeller input is not so much affected by the differential pressure.

When the drain valve is open, the impeller input decreases remarkably. In this case, however, the input power is greatly affected by the differential pressure, and increases rapidly with increase in the leakage flow from the gates. Therefore, to minimize the water leaked from the gates by reducing the spiral casing pressure is very effective for the reduction of starting input power when the drain valve is open. Figure 27 shows a photo indicating the impeller rotating in the air when the runner band drain valve is closed. Leaked water accumulates in the priming chamber and enters the impeller (whitish cloudy portion in photo). Particularly heavy water intrusion is observed along the H.P.S. of vanes. Part of the water flows through the impeller along the inner wall of band near the L.P.S. side into the draft tube.

Figure 28 shows a photo when the drain valve is open. Priming chamber appears semi-transparent in the photo due to lack of water accumulation. Though a slight amount of water may enter along the H.P.S. of impeller vanes, no water passes through the impeller along the L.P.S. side. All leaked water passes through the outer peripheral gap of impeller to flow out through the drain holes in the runner band chamber.

2. Air exhausting and water filling

When the impeller reaches the rated speed and the generator-motor is synchronized, the air exhaust valve is opened to release air around the impeller and fill the water. If the air exhaust system is not properly designed, the exhaust may be stagnant[9]. To prevent stagnation of air exhaust in the prototype pump-turbine, the optimum exhaust system should be determined in advance by observing the phenomena up to the establishment of priming pressure in the model test.

Figure 29 illustrates the time sequential variations of priming pressure, impeller input and axial thrust during the air exhausting and water filling process. Figures 30 through 34 show the the phenomena in sequence. When the air exhaust valve is opened, the depressed water level (Fig. 30) rises to reach the impeller vane bottom end (Fig. 31). Water is spooned up by vanes and is filled along the inner wall of band to the priming chamber under the pure centrifugal action (Fig. 32). In this process, the drawn water replaces the air without mixing with it and stable water filling

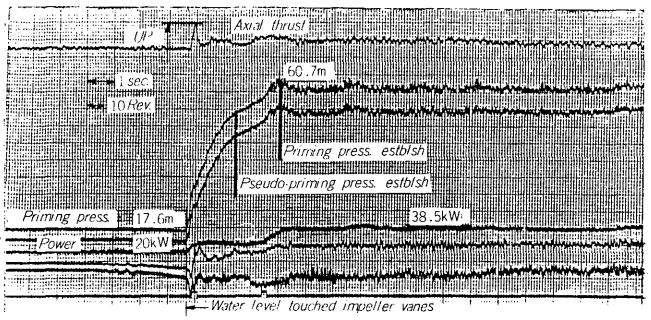

Fig. 29 Priming pressure establishes

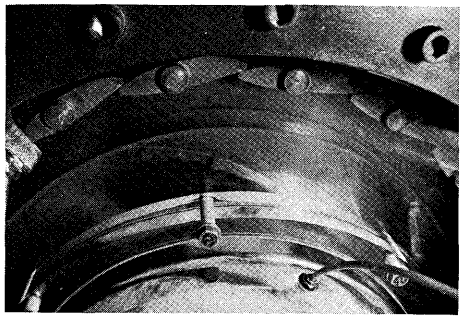

Fig. 32 Water filling in the priming chamber

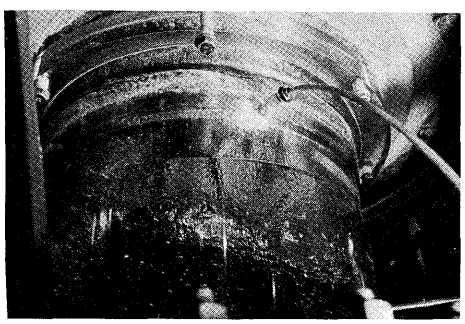

Fig. 30 Water depression

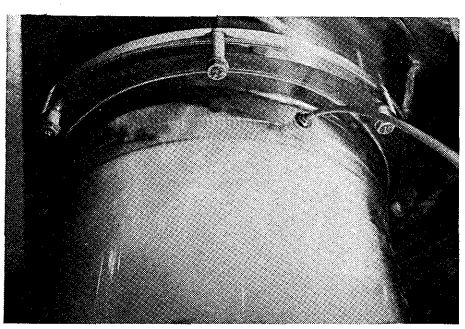

Fig. 33 Reverse flow

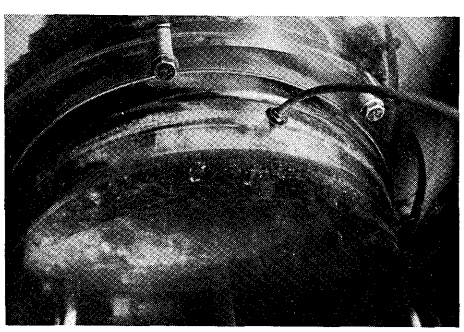

Fig. 31 Water touches vanes

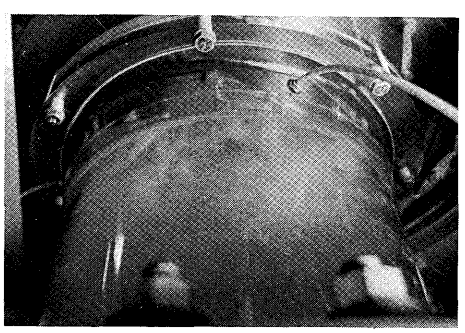

Fig. 34 Water filling finishes

proceeds smoothly. During the course, the priming pressure increases linearly (Fig. 29). This process continues till water fills the channels between vanes outside the impeller eye diameter. And the water level stops at the bottom end of impeller vanes without rising anymore.

The moment water reaches the eye diameter after filling up the channels along the band inner wall under the pure centrifugal action, the water level rises suddenly. In that instant, the impeller starts sucking water from the crown side under the hydrodynamic pumping action, and the reverse flow occurs on the band side. In this condition, air remaining inside of eye diameter mixes with water violently. Reverse flow at the impeller inlet increases its vehemence and the air-entrained reverse flow reaches the upper draft tube (Fig. 33). From the exhaust holes, the air-water mixture is released and the air exhausting speed drops suddenly. This causes the folding of priming pressure curve (Fig. 29), establishing the "pseudo-priming pressure".

While the water is being filled under the pure centrifugl action, the impeller input power remains constant at a low level. When the flow pattern changes to produce the hydrodynamic pumping action, the input power increases rapidly because of enormous energy consumption required to reverse the sucked water toward upstream side. As the exhaust proceeds further (Fig. 34), both the input power and priming pressure rise. With the completion of exhaust and filling, the shut-off operation is reached. As is evident from the above description, the more the air exhaust is achieved by the time the water filling reaches the eye diameter under the pure centrifugal action, the less the residual air and water are mixed under the hydrodynamic pumping action, and thus a smoother air exhaust and water filling can be achieved.

VIII. Conclusion

It is rather expensive and time consuming to perform a

visual observation of internal flow pattern through a model pump-turbine together with measuring the static and dynamic performance characteristics. This drawback can well be offset by the possibility of recognizing and evaluating the flow stability in terms of not only the cavitation and vortex core, but also the flow separation, dead water zone, rotating stall and vortex string on the boundary between normal and reverse flows. The visual observation accompanied by the performance test as well as the computerized flow analyses may, therefore, well contribute to an exact evaluation of hydraulic characteristics of a pump-turbine (origin of efficiency drop, reason for the increase in dynamic performance such as pressure pulsations and fluctuations of gate torque, axial and radial thrust). This in turn helps in predicting the operating conditions of a prototype pump-turbine more precisely, and makes the model test more meaningful.

References:

[1] T. Kubota, "Hydraulic Characteristics of Francis Pump-Turbine", Fuji Jiho **40-4** (1967), pp. 257-264 (in Japanese).

[2] T. Ueda, T. Kubota and H. Aoki, "Vibration Reduction of Reversible Pump-Turbines", Fuji Electric Review **19-4** (1973), pp. 136-145.

[3] T. Kubota and H. Matsui, "Application Limits of Francis Reversible Pump-Turbine to Hydro-Plant with Large Head Variation", Fuji Electric Review **22-2** (1976), pp. 65-71.

[4] T. Kubota, S. Takimoto and H. Aoki, "Depelopment of Model Turbine by Computerized Numerical Experiments", Fuji Electric Review **23-2** (1977), pp. 66-71.

[5] L. Pulpitel, Discussion for XI/2, 7th-IAHR-Symposium, Wien (1974), Trans. Part 2, pp. 298-299.

[6] T. Kubota and H. Matsui, "Cavitation Characteristics of Forced Vortex Core in the Flow of the Francis Turbine", Fuji Electric Review **18-3** (1972), pp. 102-108.

[7] T. Kubota and H. Aoki, "Pressure Surge in the Draft Tube of Francis Turbine," IAHR/IUTAM - Symposium on Practical Experiences with Flow Induced Vibration, Karlsruhe (1979), Preprient 2,

[8] M. Nishi, T. Kubota, S. Matsunaga and Y. Senoo, "Study on Swirl Flow and Surge in an Elbow Type Draft Tube", 10th - IAHR - Symposium, Tokyo (1980), Proceedings Vol. 1, pp. 557-568.

[9] M. Okada, "Various Hydraulic Problems in the Field Operation of Recent Pump-Turbines", Turbo-Machinery **4-1** (1976), pp. 36-42 (in Japanese).